

Observation of edge solitons and transitions between them in a trimer circuit lattice

Rujiang Li^{1,*}, Xiangyu Kong¹, Wencai Wang¹, Yixi Wang¹, Yongtao Jia¹, Huibin Tao^{2,†}, Pengfei Li^{3,4}, Ying Liu¹, and Boris A. Malomed^{5‡}

¹*National Key Laboratory of Radar Detection and Sensing,*

School of Electronic Engineering, Xidian University, Xi'an 710071, China

²*School of Software Engineering, Xi'an Jiaotong University, Xi'an, China*

³*Department of Physics, Taiyuan Normal University, Jinzhong, 030619, China*

⁴*Institute of Computational and Applied Physics,*

Taiyuan Normal University, Jinzhong, 030619, Shanxi, China and

⁵*Instituto de Alta Investigación, Universidad de Tarapacá, Casilla 7D, Arica, Chile*

In nonlinear topological systems, edge solitons either originate from linear topological edge modes or emerge as nonlinearity-induced localized states without topological protection. While electric circuits (ECs) provide a platform for realizing various types of topological insulators, observation of edge solitons and transitions between them in EC lattices remains a challenging problem. Here, we realize quench dynamics in nonlinear ECs to experimentally demonstrate both topologically nontrivial and trivial edge solitons in a trimer EC lattice and transitions between them. In the weakly nonlinear regime, we observe two types of topologically nontrivial edge solitons that originate from the corresponding linear topological edge states, characterized by the presence of mutually antisymmetric or symmetric peaks at two edge sites. Under strong nonlinearity, topologically trivial edge solitons with antisymmetric, symmetric, and asymmetric internal structures are discovered. The work suggests possibilities for exploring sophisticated nonlinear states and transitions between them in nonlinear topological systems.

Introduction

Topological insulators (TIs) are media that act as conventional insulators in the bulk but maintain conductivity on their surfaces, provided by topologically protected edge states [1–6]. Counterparts of TIs have been realized across diverse physical platforms, including acoustic and mechanical ones [7–11], bosonic condensates in ultracold gases [12], and photonics [13–16], the immunity of topological edge states to local deformations and disorder being crucial for promising potential applications. Further, the interplay between the topological structure of optical media and their intrinsic nonlinearity [17, 18] leads to the creation of edge solitons, which originate from the linear topological edge states and inherit their topological protection [19–38]. In addition to the topologically nontrivial edge solitons, conventional ones, which are nonlinearity-induced localized states at the edge of a bulk optical waveguide, have also been discovered in nonlinear photonic topological insulators [21, 31, 32, 35, 39]. The conventional edge solitons are considered as topologically trivial states, since they do not originate from linear topological edge modes. However, historically, they have been referred to as surface solitons and regarded as important members of the soliton family [40–42]. It is relevant to mention that trivial edge solitons emerge with the power exceeding a certain finite threshold value [31, 37, 40, 43].

Electric circuits (ECs) have been widely used as a versatile platform for simulations of a great variety of nonlinear modes which are known in other areas of physics [44]. In particular, this platform was recently proposed as a means for emulating various types of TIs [45–52]. In this context, owing to the broad flexibility in constructing

EC lattices and employing site-resolved, phase-resolved, time-resolved, and frequency-resolved measurement techniques, ECs have demonstrated their relevance for exploring multidimensional [53, 54], higher-order [55, 56], non-Hermitian [57–61], non-Abelian [62, 63], and non-Euclidean TIs [64, 65]. While some work on nonlinear topological ECs has been reported [66–72], these studies typically rely on driving the lattices with continuous voltage sources. This approach works well in simple systems, but becomes cumbersome when applied to the study of nonlinear topological lattices which exhibit a broad variety of solitons, as it necessitates additional considerations such as taking care of bistability [23, 24, 35, 73]. Due to the lack of a suitable realization scheme that can selectively excite the desired nonlinear states, the observation of edge solitons in EC lattices remains a significant challenge – particularly, transitions between topologically nontrivial and trivial edge solitons, as well as transitions between different types of topological states [74].

In this work, we have experimentally implemented a nonlinear trimer EC lattice with a linear topological structure, observing both topologically nontrivial and trivial edge solitons, using the technique of quench dynamics. We measure the time evolution of site voltages initiated by the out-of-phase, in-phase, and single-site excitations, while tuning the EC nonlinearity by the excitation voltage. For the out-of-phase and in-phase excitations, we consider both weak and strong nonlinearity. Under the weak nonlinearity, the excitation creates topologically nontrivial edge solitons originating from the linear topological edge states. In contrast, under the action of strong nonlinearity, the initial voltage distribution leads to the creation of conventional

edge solitons, thus indicating that a transition from topologically nontrivial to trivial edge solitons occurs with the growth of the nonlinearity strength. We also explore the cases of both weak and strong nonlinearity for single-site excitations. For weak nonlinearity, voltage oscillations are observed due to the overlap of two types of linear topological edge states. When the excitation voltage exceeds a threshold value, strong voltage localization around a single edge site occurs, forming a topologically trivial asymmetric edge soliton. The discovery of the three types of topologically trivial edge solitons was not reported in the previous study of a nonlinear trimer photonic array [37]. This work offers a general approach to the creation of solitons in EC lattices, which may be also helpful for the complete understanding of exotic self-trapped states and phase diagrams in more complex nonlinear topological systems.

Results

Implementation of a nonlinear trimer EC lattice and the realization of quench dynamics. Although the Su-Schrieffer-Heeger lattice is the prototypical model of a topological lattice, we here investigate a one-dimensional trimer lattice with onsite nonlinearity, to highlight the powerful capabilities of quench dynamics. We will show that, in contrast to the nonlinear Su-Schrieffer-Heeger lattice [31], the nonlinear trimer lattice supports a diverse range of edge solitons, both topologically nontrivial and trivial ones being effectively excited and probed through phase-resolved techniques.

As shown in Fig. 1a, the nonlinear trimer lattice is governed by the following dynamical equations:

$$i \frac{d\psi_n^A}{dt} = E(\psi_n^A) \psi_n^A + J' \psi_{n-1}^C + J \psi_n^B, \quad (1)$$

$$i \frac{d\psi_n^B}{dt} = E(\psi_n^B) \psi_n^B + J \psi_n^A + J \psi_n^C, \quad (2)$$

$$i \frac{d\psi_n^C}{dt} = E(\psi_n^C) \psi_n^C + J \psi_n^B + J' \psi_{n+1}^A. \quad (3)$$

Here, J and J' are the intra- and inter-cell hopping amplitudes, respectively, and $E(\psi_n^{A,B,C})$ are the onsite energies which depend on the respective wave functions. To analyze the properties of the states in the lattice, a common approach is to study the quench dynamics by defining an initial state $\psi_n^{A,B,C}(t=0)$ and exploring its time evolution [22, 27, 36]. Note that the quench dynamics defined here refers to the general dynamical behavior of a prepared initial state, which is distinct from the oscillation quenching observed in systems of coupled nonlinear oscillators, specifically including the oscillation-death and amplitude-death behaviors [75–79]. In optical waveguide arrays, the quench dynamics we refer to is typically investigated by replacing the time dimension with an extra spatial dimension [19–21, 28, 30, 32, 37].

We implement the above model including the quench dynamics using the nonlinear EC lattice shown in Fig.

1b. Each unit cell includes three nonlinear LC resonators with inductor L_g , capacitors C_A or C_B , and common-cathode diodes C_v , with capacitance $C_v = C_L / (1 + |v/v_0|)^M$, where C_L , v_0 , and M are constants, and v is the amplitude of the voltage applied to terminals of the common-cathode diode (the model of this element is presented in Supplementary Note 1). The nonlinear resonators are coupled via capacitors $C_{1,2}$. The four types of capacitors satisfy the relation: $C_A - C_B = C_1 - C_2$. In the two leftmost resonators, single-pole double-throw (SPDT) switches control the charging and discharging of the respective capacitors $C_{A,B}$ and diodes C_v .

From the EC schematic and illustration of quench dynamics shown in Figs. 1b and c, respectively, it is seen that, when the SPDT switches are connected to the DC voltage sources, capacitors $C_{A,B}$ and diodes C_v are charged to constant voltages $V_{DC}^{A,B}$. The charging operation corresponds to the preparation of the initial state. When the SPDT switches are simultaneously toggled to the circuit nodes, the instantaneous voltages at the two leftmost circuit nodes are given by $\psi_1^A = V_{DC}^A$ and $\psi_1^B = V_{DC}^B$, while all other nodes have zero voltage. This moment is recorded as $t = 0$. It is worth noting that the phase of the initial state can be adjusted using the DC voltage sources.

At $t > 0$, the charged capacitors and diodes discharge. Under the slowly-varying envelope approximation, which is ensured by the conditions $C_{1,2} \ll C_A + C_L$ and $C_L - C_v \ll C_A + C_L$ (see the parameters for circuit components in Methods, Sample fabrication and measurement), the time evolution of the initial voltage distribution is governed by equations that take the same form as Eqs. (1)-(3) (for the derivation of the EC equations, see Supplementary Note 1; for the detailed implementation of the quench dynamics, refer to Methods, Sample Fabrication and Measurement, and Supplementary Note 1). In contrast to previous work that begins with the Lagrangian [66], we present an ab initio derivation starting from the Kirchhoff circuit equations. These time-dependent equations are fundamental for conducting the study of quench dynamics.

From the expressions $J_{1,2} = \frac{C_{1,2}}{2(C_A + C_L)} \omega_0$ with $\omega_0 = \frac{1}{\sqrt{L_g(C_A + C_L)}}$ as the carrier frequency (see Supplementary Note 1 for these definitions), the intracell and intercell hopping amplitudes J and J' are related to the coupling capacitors C_1 and C_2 , respectively. The onsite energies are expressed as $E(\psi_n^{A,B,C}) = E_0 + g(\psi_n^{A,B,C})$, where $E_0 = \left[1 - \frac{C_1 + C_3}{2(C_A + C_L)}\right] \omega_0$ is a constant term, and $g(\psi_n^{A,B,C}) = \frac{C_L - C_v(\psi_n^{A,B,C})}{2(C_A + C_L)} \omega_0$ represents the voltage-dependent terms. The wave functions $\psi_n^{A,B,C}$ are defined as the complex amplitudes of the temporal voltages $V_n^{A,B,C}(t)$, i.e., $V_n^{A,B,C}(t) = \frac{1}{2} \psi_n^{A,B,C}(t) + \text{c.c.}$ Under these correspondences, the resonant frequencies of

the EC lattice correspond to the frequency spectra of the nonlinear trimer lattice.

Figure 1d shows the experimental sample of the nonlinear trimer EC lattice, with the inset zooming in a fragment containing the typical circuit components (see the sample design and fabrication in Methods, Sample fabrication and measurement). Note that, in our experiments, we use two common-cathode diodes connected in parallel to provide the desired capacitance C_v .

Frequency spectra and profiles of edge solitons.

In the linear regime, which is realized for an infinitesimal amplitude of wave functions when $\psi_n^{A,B,C}$ approach zero, the trimer EC lattice exhibits three dispersive bands separated by two finite bandgaps under periodic boundary condition (see Supplementary Figure S5 and relevant discussion in Supplementary Note 2). The linear trimer lattice being inversion-symmetric, i.e., $PH(k)P^{-1} = H(-k)$, with Hamiltonian in the reciprocal space $H(k)$ and inversion operator P , the Zak phase, defined as the integral over the Brillouin zone, $\mathcal{Z} = i \int_{\text{BZ}} \langle \psi_k | \frac{\partial}{\partial k} | \psi_k \rangle dk$, is quantized, taking solely values 0 or π (modulo 2π). When the intracell hopping J is smaller than its intercell counterpart J' , the linear trimer lattice is topologically nontrivial with $\mathcal{Z} = \pi, 0$, and π for the bottom, middle, and top bands, respectively. According to the bulk-boundary correspondence, for the trimer lattice with a finite number of unit cells, one pair of edge states appear in each topological bandgap [80–84]. Due to the inversion symmetry of the trimer EC lattice, the edge states in the bottom topological gap exhibit the largest magnitudes at the two outermost sites, but with opposite signs, resulting in antisymmetric internal structures (see discussion in Supplementary Note 2). In contrast, the edge states in the top topological bandgap also show the largest magnitudes at the two outermost sites, but with the same sign, leading to symmetric internal structures.

In the nonlinear regime, to give a better physical insight into the existence of edge solitons, we first move to the continuum limit, where $\psi_n^{A,B,C} \rightarrow \psi_{A,B,C}(x)$, with x representing the continuum limit index. We investigate the evolution of solution trajectories with respect to x through a phase-space analysis of nonlinear systems [26, 66, 85]. This approach allows us to predict that edge solitons exist in a semi-infinite trimer lattice under both weak and strong nonlinearity (for a detailed discussion on equilibrium points and solution trajectories, see Supplementary Figures S7 and S8, and Supplementary Note 3). In the weakly nonlinear regime, we identify two types of solutions. One type exhibits $\psi_A(x) \approx -\psi_B(x)$ and $\psi_C(x) \approx 0$, which corresponds to the antisymmetric internal structure. The other type shows $\psi_A \approx \psi_B$ and $\psi_C \approx 0$, which corresponds to the symmetric internal structure. Both types of solutions decay monotonically

as one moves away from the lattice boundary. In contrast, in the strongly nonlinear regime, assuming $\psi_C \approx 0$, we predict the existence of two types of solutions with nearly antisymmetric and symmetric internal structures, respectively, as well as a class of solutions characterized by strongly asymmetric profiles, where $\psi_A \gg \psi_B$.

We then numerically solve Eqs. (1)-(3) and the calculated voltage-dependent frequency spectra are displayed in Fig. 2a (see the numerical method in Methods, Theoretical calculations). The solid curves represent the edge solitons. For comparison, the underlying frequency spectra of the linear bulk bands are denoted as the shaded regions. The three bandgaps, *viz.*, the semi-infinite gap, top topological gap, and bottom topological gap, are defined with respect to the linear bulk spectra. We use the voltage at the leftmost site, ψ_1^A , to characterize the strength of the EC nonlinearity. Without the loss of generality, we focus on the edge solitons located at the left edge of the trimer EC lattice.

Under weak nonlinearity, as indicated by the two purple curves commencing from $\psi_1^A = 0$, the topologically nontrivial edge solitons originate from the linear topological edge states. Inheriting the internal structures from the parent linear states, from the voltage distributions, the nontrivial edge solitons in the bottom and top topological gaps exhibit the nearly antisymmetric and symmetric peaks at the two leftmost sites, respectively [see profiles of states (1) and (2) in Fig. 2b]. For comparison with other types of edge solitons that will be introduced later, we refer to states (1) and (2) as antisymmetric and symmetric nontrivial edge solitons, respectively. These two types of nontrivial edge solitons are coincident with the solutions under weak nonlinearity in the continuum limit.

As ψ_1^A increases, the nontrivial edge solitons, i.e., states (1) and (2), become delocalized, entering the linear bulk bands [37] (see Supplementary Figures S9-S11 for complete frequency spectra and Supplementary Note 4 for detailed discussion). However, as indicated by the blue curves, families of edge solitons emerge in the top topological bandgap and semi-infinite one [see states (3)-(5) and the corresponding branches], being completely separated from the branches of states (1) and (2) [37]. These edge solitons are weakly localized, especially when they are in the vicinity of the band edges of the linear bulk states. States (3) and (4) exhibit the antisymmetric internal structures from their voltage distributions, while state (3) exists only in a narrow region of the top topological gap, becoming delocalized upon entering the linear bulk band. Although the branch for state (5) is close to that of the symmetric nontrivial edge solitons [state (2)], it displays a strongly asymmetric profile at the two leftmost sites. Based on the internal structures, states (3), (4), and (5) in Fig. 2b are labeled as “antisymmetric”, “symmetric”, and “asymmetric”, respectively.

When the nonlinearity becomes sufficiently strong,

self-sustained states emerge at the edge of the trimer lattice, where the nonlinearity dominates over the lattice couplings. From the voltage distributions, states (6)-(8) in Fig. 2b show typical profiles of the three types of edge solitons, featuring antisymmetric (staggered), nearly symmetric (unstaggered), and asymmetric (strongly confined) internal structures, respectively. These edge solitons are conventional self-trapped topologically trivial modes [40–43]. We refer to states (6)-(8) as antisymmetric, symmetric, and asymmetric trivial edge solitons, respectively. Due to their fundamentally different physical origins, the branches corresponding to these topologically trivial edge solitons are completely isolated from those of the nontrivial edge solitons [31]. Note that the existence of these nontrivial edge solitons validates the prediction produced by the phase-space analysis.

Among all the edge solitons shown in Fig. 2b, the topologically trivial ones (6)-(8), which exist in the semi-infinite gap, exhibit the strongest exponential localization with the voltage distribution concentrated almost entirely at the two leftmost sites [or solely at the first leftmost site, for state (8)]. On the other hand, the topologically nontrivial edge solitons labeled (1)-(2) in Fig. 2b feature slowly decaying oscillatory tails. These features indicate the existence of a nonlinearity-induced transition from topologically nontrivial edge solitons to trivial ones [39]. Additionally, we note that the frequency spectra shown in Fig. 2a are concentrated around the carrier frequency ω_0 . Therefore, the slowly-varying envelope approximation, used to derive equations similar to Eqs. (1)-(3) is valid, provided that the voltages are not excessively large.

Observation of edge solitons and transitions between them. To experimentally investigate the topologically nontrivial and trivial edge solitons and the transitions between them, we implement quench dynamics in the nonlinear trimer EC lattice. Following the scheme shown in Figs. 1b and c, we create the input with $\psi_n^{A,B,C}(t=0)$ to match the expected internal structure of the edge solitons. Specifically, for the antisymmetric and symmetric cases, we set $V_{DC}^A = -V_{DC}^B = \psi_0$ and $V_{DC}^A = V_{DC}^B = \psi_0$, respectively. This indicates that the initial voltages are out of phase and in phase, respectively. For the asymmetric edge solitons, we set $V_{DC}^A = \psi_0$ and $V_{DC}^B = 0$, meaning that only the first leftmost site is excited. Although multiple edge solitons are present in Fig. 2, only the one that matches the initial input distribution and is dynamically stable can be effectively excited. Under an input excitation, we record the voltage distributions in the EC lattice at various time intervals. If a steady state is achieved, the voltage distribution will correspond to an eigenstate. This allows us to identify which of the independent edge solitons is being excited. Similar to optical waveguide arrays, where nonlinearity is

influenced by optical power [37], the nonlinearity in the EC lattice is governed by the value of ψ_0 .

In the case of out-of-phase excitations, we present the experimentally measured and theoretically calculated temporal evolution of the site voltages, represented by the magnitudes of the complex amplitudes, $|\psi_n^{A,B,C}|$, in Figs. 3a and b, respectively (see the method for theoretical calculations in Methods, Theoretical calculations). For $\psi_0 = 0.02$ V, i.e., under weak nonlinearity, the stability of the antisymmetric nontrivial edge solitons (see Supplementary Note 4 for the stability analysis) and substantial overlap between the initial voltage distribution and state (1) shown in Fig. 2 enable the system to achieve a steady state, before the voltages decay to undetectable levels due to the dissipative losses from the circuit components. Thus, we observe the formation of the antisymmetric nontrivial edge soliton. For $\psi_0 = 2.5$ V (strong nonlinearity), a steady state is also achieved and we observe the formation of state (6) shown in Fig. 2, which represents the antisymmetric trivial edge soliton with strong localization. This outcome results from the nearly perfect overlap between the initial voltage distribution and established soliton profiles, along with the stability of these solitons across a broad voltage range.

For medium nonlinearity strengths, corresponding to $\psi_0 = 0.2, 0.5, 0.65$, and 1.2 V, steady states are not achieved under the excitations, although the two leftmost sites still exhibit the highest voltage. When the excitation voltage corresponds to a delocalized state or a strongly unstable edge soliton, the voltage still localizes at these two sites due to limited measurement time (See Supplementary Figure S12 and Supplementary Note 5). If the excitation voltage corresponds to a weakly unstable edge soliton, the initial voltage may excite it, but the localized voltage eventually collapses.

To compare with the above results, we also study a trimer EC lattice with $J > J'$, which, as mentioned above, is topologically trivial in the linear limit. We observe voltage diffraction accompanied by local oscillations across the entire range of excitation voltages, indicating that steady states are never established under varying excitations. This observation confirms the absence of both topologically nontrivial and trivial edge solitons with an antisymmetric internal structure (see Supplementary Figure S14 and Supplementary Note 6). Note that the trivial edge solitons do not exist in this case because the circuit lattices exhibit saturable nonlinearity, and the nonlinearity strength is insufficient to induce mode localization.

To characterize the excitation of antisymmetric edge solitons during quench dynamics, we define the state localization S_2 as follows:

$$S_2 = \frac{|\psi_1^A|^2 + |\psi_1^B|^2}{\sum_n (|\psi_n^A|^2 + |\psi_n^B|^2 + |\psi_n^C|^2)}. \quad (4)$$

It measures the voltages of the two leftmost sites relative to the total voltage across all EC nodes. Additionally, we introduce the asymmetry parameter Θ to quantify the imbalance between the voltages at these two sites:

$$\Theta = \frac{|\psi_1^A| - |\psi_1^B|}{|\psi_1^A| + |\psi_1^B|}. \quad (5)$$

Theoretically, the state localization and asymmetry parameter should be evaluated after a sufficiently long evolution time. Due to the inevitable circuit dissipations in experiments, we extract the voltage distributions at $t = 45 \mu\text{s}$, with the corresponding results for the state localization and asymmetry parameter shown in Fig. 3c. We will demonstrate below that the selection of this time moment is appropriate for observing the nonlinearity-induced transition between the topologically nontrivial and trivial edge solitons.

The continuous curves and chains of circles in Fig. 3c represent the theoretical and experimental results, respectively. Although the circuit dissipation causes deviation in the specific values of the experimental results, the overall trends well agree with the theoretical predictions. The state localization is relatively high near $\psi_0 = 0$ and at $\psi_0 > 2$, as the topologically nontrivial and trivial edge solitons are formed under the weak and strong nonlinearity, respectively. Notably, the trivial edge solitons [such as state (6) in Fig. 2] are, generally, localized stronger than the nontrivial ones [such as state (2)], resulting in $S_2 \approx 1$ for $\psi_0 > 2.5$ V. This fact indicates the above-mentioned nonlinearity-induced transition from the weakly nonlinear nontrivial edge solitons to the trivial ones supported by strong nonlinearity [39]. Note that the same conclusion can be reached by evaluating the inverse participation ratios (IPRs) of the voltage distributions as nonlinearity increases (see Supplementary Figure S17 and Supplementary Note 7 for the results of IPRs). The IPR is defined as follows:

$$\text{IPR} = \frac{\sum_n (|\psi_n^A|^4 + |\psi_n^B|^4 + |\psi_n^C|^4)}{\left[\sum_n (|\psi_n^A|^2 + |\psi_n^B|^2 + |\psi_n^C|^2) \right]^2}. \quad (6)$$

Besides, throughout this transition, the antisymmetric internal structure of the edge soliton is preserved, with the asymmetry parameter Θ remaining close to zero, as shown in Fig. 3c. Phase measurements further support this observation (see Supplementary Figure S18 and Supplementary Note 8 for the phase measurement of the edge solitons).

Similarly, we investigate the evolution of site voltages initiated by in-phase excitations. As shown in Figs. 4a and b, the formation of the symmetric nontrivial edge soliton [state (2) in Fig. 2] is observed in the case of weak nonlinearity with $\psi_0 = 0.02$ V, again attributed to the stability of the topologically nontrivial edge soliton and

significant overlap of the excitation distribution with the soliton profile (see Supplementary Figure S9 and Supplementary Note 4). In the case of a medium nonlinearity strength, the two leftmost sites display the highest voltage due to the limited measurement time. For a longer evolution time, voltage diffraction or oscillations occur, if the excitation corresponds to a delocalized state or unstable edge soliton (see Supplementary Figure S10 and Supplementary Note 4). Even for $\psi_0 = 2$ V, in the regime of strong nonlinearity, the topologically trivial edge soliton [state (7) in Fig. 2] can only be observed briefly, before evolving into the asymmetric one [state (8)] due to the instability. Note that the voltage values in the regime of the strong nonlinearity differs from those in Figs. 3a-b, as the symmetric trivial edge solitons can exist under smaller nonlinearities compared to the antisymmetric ones (see Fig. 2). For the trimer EC lattice with $J > J'$, voltage diffraction is observed throughout the entire parameter range, indicating the absence of both symmetric nontrivial and symmetric trivial edge solitons (see Supplementary Figure S15 and Supplementary Note 6).

We again evaluate the state localization and asymmetry parameter using the voltage distributions at $t = 45 \mu\text{s}$. In Fig. 4c, the enhanced state localization indicates a transition from weakly nonlinear nontrivial edge solitons to strongly nonlinear trivial ones, and the nearly zero values of the asymmetry parameter imply the preservation of the symmetric internal structure of the edge solitons (also see Supplementary Figure S18 and Supplementary Note 8 for the phase measurements). The discrepancies between the experimental results (represented by chains of circles) and their theoretical counterparts (shown as continuous curves), particularly in the medium-nonlinearity regime, are explained by effects of the circuit dissipation in the experiment.

To further clarify the differences between the topologically nontrivial and trivial edge solitons, we study the quench dynamics initiated by the single-site excitations applied exclusively to the first leftmost site. In Figs. 5a and b, one observes voltage oscillations between the two leftmost sites in the case of weak nonlinearity. These oscillations are induced by the overlap of the excitation with the linear antisymmetric and symmetric topological edge states (see Supplementary Figure S10 and Supplementary Note 4). In the case of medium nonlinearity strength, the asymmetric edge soliton [state (5) in Fig. 2] does not form due to its strong instability and weak localization (see Supplementary Figure S10 and Supplementary Note 4). However, when the nonlinearity is sufficiently strong, such as when $\psi_0 = 2$ V, the steady state is achieved and we observe the formation of the asymmetric trivial edge soliton [state (8)]. Note that we use the same voltage value for the regime of strong nonlinearity as in Figs. 4a-b, since the symmetric and asymmetric trivial edge solitons require comparable nonlinearity strengths

for their existence (see Fig. 2).

This observation is further verified by a modified definition of the localization parameter,

$$S_1 = \frac{|\psi_1^A|^2}{\sum_n (|\psi_n^A|^2 + |\psi_n^B|^2 + |\psi_n^C|^2)}, \quad (7)$$

cf. Eq. (4). As shown in Fig. 5c, when ψ_0 is close to zero, the localization is weak due to voltage oscillations. In contrast to that, we find that $S_1 \approx 1$ for $\psi_0 > 2$ V, featuring a significant enhancement in the state localization. Here too, the discrepancy between the experimental results (represented by the chain of circles) and their theoretical counterparts (depicted by the continuous curve) is explained to the effect of the circuit dissipation in the experiment. In particular, in the regime of the medium nonlinearity, such as the one with $\psi_0 = 1.2$ V, the experimental results deviate because the asymmetric trivial edge soliton is not excited due to its weak localization in this specific regime. The overall trends of the experiential and theoretical results indicate that there are no weakly-nonlinear asymmetric nontrivial edge solitons, while strongly-nonlinear asymmetric trivial ones do exist. Note that asymmetric edge solitons, including both the nontrivial and trivial ones, do not exist in the trimer EC lattice with $J > J'$ (see Supplementary Figure S16 and Supplementary Note 6).

Discussion

The edge solitons and nonlinearity-induced transitions observed in our work are fundamentally distinct from the nonlinearity-induced topological phase transitions reported previously [66, 68]. In those studies, the EC lattice is topologically trivial in the linear limit. Under strong excitation, the lattice transitions to a topologically nontrivial phase that supports topologically nontrivial edge states. In other words, as the excitation strength decreases, these nontrivial edge states reduce to linear trivial bulk states, rather than linear topological edge states. In contrast, we develop the technique of quench dynamics and demonstrate the existence of both topologically nontrivial and trivial edge solitons. Specifically, the nontrivial edge solitons directly arise from the linear topological edge states. Furthermore, we observe the transitions from topologically nontrivial to trivial edge solitons with enhanced nonlinearity. These features were not reported in previous works [66, 68].

On the other hand, while both topologically nontrivial and trivial edge solitons are important members of the soliton family in a nonlinear topological lattice, trivial edge solitons are usually overlooked [19, 20, 22–25, 27–30, 37, 38]. Notably, Leykam *et al.* proposed edge solitons that originate from the linear topological edge states in a topologically nontrivial lattice, as well as self-induced nonlinear edge modes in a topologically trivial lattice [20]. They did not study the conventional trivial edge

solitons in a nontrivial lattice. Similar to our work, Kartashov *et al.* also studied a nonlinear trimer lattice and observed the topologically nontrivial edge solitons [37]. However, the topologically trivial edge solitons residing in the semi-infinite gap have not been explored. The enhanced localization associated with increased nonlinearity, which is an essential signature of the existence of trivial edge solitons and the transition from topologically nontrivial to trivial edge solitons, was not revealed in their experiments.

Very recently, Sone *et al.* theoretically introduced the concept of the nonlinear Chern number, which is used to characterize the nonlinear Chern insulators and nonlinearity-induced topological phase transition [86]. In contrast to this work, we explore both the regimes of weak and strong nonlinearity of a lattice which is topologically nontrivial in the linear limit. In addition to the topologically nontrivial edge solitons that exist under weak nonlinearity and originate from the linear topological edge states, we also experimentally identify the topologically trivial edge solitons under strong nonlinearity and establish the nonlinearity-induced transition between the nontrivial and trivial edge solitons.

The coexistence of topologically nontrivial and trivial edge solitons has been experimentally confirmed in two photonic settings [32, 35]. Compared with these realizations, our platform of nonlinear EC lattices offers several advantages. First, we can construct more complex nonlinear topological systems using EC lattices and explore exotic self-trapped states through the technique of quench dynamics. Second, the platform of nonlinear EC lattices has the ability of phase-resolved measurements. We additionally provide more experimental evidence of the existence of edge solitons (see Supplementary Figure S18 and Supplementary Note 8 for the phase measurements of the edge solitons). Finally, due to the broad availability of circuit components, lattices exhibiting multiple types of nonlinearities can be built [44, 72]. For instance, the value of M in the formula $C_v = C_L / (1 + |v/v_0|)^M$ can be adjusted by employing diodes with different parameters. This flexibility suggests one to explore more complex nonlinearities in EC lattices, in addition to the typical cubic (Kerr) nonlinearity dealt with in conventional nonlinear optics [17, 18, 87].

Conclusion

In this work, we have realized the quench dynamics in the nonlinear trimer EC lattice with tunable nonlinearity, observing the time evolution of site voltages initiated by different excitations. We have experimentally identified the weakly-nonlinear antisymmetric and symmetric nontrivial edge solitons, as well as the strongly-nonlinear trivial edge solitons featuring antisymmetric, symmetric, and asymmetric internal structures. We have found the nonlinearity-induced transition between the

topologically nontrivial and trivial edge solitons. Our findings pave the way for further exploration of nonlinear topological physics in EC lattices, suggesting insights into the interplay of topology and nonlinearity in the general context.

Methods

Sample fabrication and measurement. To ensure the observation of the edge solitons, the circuit components should have minimal parasitic parameters, and their tolerance should be as low as possible. For this purpose, we utilized capacitors ($C_A = 380$ pF, $C_B = 760$ pF, $C_1 = 180$ pF, and $C_2 = 560$ pF) with low ESL and $\pm 1\%$ tolerance. We also employed inductors with magnetic shielding and low DCR ($L_g = 15$ μ H), and carefully selected the components using an LCR meter (HIOKI IM3536). The tolerances for inductance and series resistance are $\pm 1\%$ and $\pm 2\%$, respectively. The average series resistance of the inductors is approximately 600 m Ω . To characterize the voltage response of the common-cathode diode (V60DM45C), we measured the C - V curves, obtaining parameter values $C_L = 8.62$ nF, $v_0 = 1.69$, and $M = 0.31$ by fitting these curves to the phenomenological formula $C_v = C_L / (1 + |v/v_0|)^M$. We employed standard PCB techniques to fabricate the EC lattice, ensuring that the inductors are sufficiently spaced to prevent mutual coupling. The PCB traces were designed with a relatively large width of 0.75 mm to accommodate high currents, and the layouts were carefully optimized to minimize parasitic parameters and coupling with other circuit components.

To implement the quench dynamics, an SPDT switch with two channels (ADG1636) was used to control the charging and discharging of capacitors $C_{A,B}$ and diodes C_v . To ensure synchronization between the two channels, one specific switch with a small parameter error of $t_{\text{ON/OFF}}$ was selected based on the measured switching times. Additionally, during the PCB design, the signal paths for the logic control inputs of both channels were deliberately designed to have equal physical lengths, effectively minimizing propagation delay skew. The capacitor C_A and diode C_v in the leftmost nonlinear LC oscillator were connected to the drain terminal of one channel of the switch, while the capacitor C_B and diode C_v in the second leftmost nonlinear LC oscillator were connected to the drain terminal of the other channel of the switch. Two independent DC voltage sources, V_{DC}^A and V_{DC}^B , were connected to the source terminals of the two channels through separate SubMiniature version A (SMA) connectors, respectively. The remaining two source terminals of the switch were each connected to the two leftmost nodes of the trimer EC lattice. The logic control inputs of the two channels were interconnected and connected to a common external digital signal generated by an arbitrary function generator (Tektronix AFG31252) via the last SMA connector on the PCB. To minimize coupling

noise and spurious signals induced by the power supplies, including both the positive and negative supplies for the switch, as well as the DC voltage sources used to charge the capacitors and diodes, we utilized DC power supplies with low ripple and noise. In addition, we implemented extra decoupling capacitors on the PCB.

When we set the external digital signal to a low voltage, the drain terminal of each channel of the switch was connected to one of the source terminals, allowing the capacitors $C_{A,B}$ and diodes C_v to charge. Once the capacitors and diodes were charged to their constant voltages, we switched the digital signal to a high voltage, connecting the drain terminal of each channel to another source terminal. This caused the capacitors $C_{A,B}$ and diodes C_v to begin discharging. We recorded the voltage signals at the EC nodes during both the charging and discharging processes using an oscilloscope that offers high vertical accuracy and low noise floor (Keysight HD304MSO). The post-processing of the recorded data, including signal capture, filtering, and Fourier analysis to extract both the amplitudes and phases of the complex amplitudes, was carried out.

Theoretical calculations. To calculate the nonlinear frequency spectra and profiles of the edge solitons, we solved the Gross-Pitaevskii equations, i.e., Eqs. (1)-(3), using the ansatz $\psi_n^{A,B,C} = \phi_n^{A,B,C} \exp(-i\omega t)$, where $\phi_n^{A,B,C}$ is the real-valued function describing the voltage distribution and ω is the frequency. We employed the Newton's method to solve the eigenvalue equation for each ω with appropriate voltage distributions adopted as the initial guesses [88]. Open boundary conditions were used to truncate the nonlinear EC lattice. Once we obtained the soliton solution at a given ω , solutions at other frequencies were obtained iteratively. The stability of the edge solitons was analyzed using the standard linear-stability technique and subsequently confirmed through simulations of the time evolution, based on the Runge-Kutta algorithm. To study the quench dynamics of the edge solitons, we also employed the Runge-Kutta algorithm for the simulations of the evolution of the initial excitations in the framework of Eqs. (1)-(3). A sufficiently small time step was used to ensure the accuracy of the simulation results.

Acknowledgements

R.L., X.K., and W.W. were sponsored by the National Key Research and Development Program of China (Grant No. 2022YFA1404902), National Natural Science Foundation of China (Grant No. 12104353), and Fundamental Research Funds for the Central Universities (Grant No. QTZX25086). P.L. was sponsored by the National Natural Science Foundation of China (11805141) and Basic Research Program of Shanxi Province (202303021211185). Y.L. was sponsored by the National Natural Science Foundation of China (NSFC) under Grant No. 62271366 and the 111 Project.

The work of B.A.M. was supported, in part, by the Israel Science Foundation through grant No. 1695/22. The numerical calculations performed in this work were supported by the High-Performance Computing Platform of Xidian University.

Author Contributions

R.L. conceived the idea. R.L., X.K., W.W., and Y.W. performed the theoretical calculations and simulations. R.L., X.K., W.W., Y.J., and H.T. designed and conducted the experiments. R.L., B.A.M., P.L., and W.W. wrote the manuscript. R.L., B.A.M., and Y.L. supervised the project.

Data availability

The data that support the findings reported in this paper are available from the corresponding authors upon reasonable request.

Code Availability

The program code used in this study is available from the corresponding authors upon reasonable request.

Competing Interests

The authors declare no competing financial interests.

* Corresponding author: rujiangli@xidian.edu.cn

† Corresponding author: coldfire2000@mail.xjtu.edu.cn

‡ Corresponding author: malomed@tauex.tau.ac.il

References

- [1] C. L. Kane and E. J. Mele, Quantum Spin Hall Effect in Graphene, *Phys. Rev. Lett.* 95, 226801 (2005).
- [2] M. König, S. Wiedmann, C. Brüne, A. Roth, H. Buhmann, L. W. Molenkamp, X.-L. Qi, and S.-C. Zhang, Quantum Spin Hall Insulator State in HgTe Quantum Wells, *Science* 318, 766 (2007).
- [3] M. Z. Hasan and C. L. Kane, Colloquium: Topological insulators, *Rev. Mod. Phys.* 82, 3045 (2010).
- [4] X.-L. Qi and S.-C. Zhang, Topological insulators and superconductors, *Rev. Mod. Phys.* 83, 1057 (2011).
- [5] F. Tang and X. Wan, Group-theoretical study of band nodes and the emanating nodal structures in crystalline materials, *Quantum Front.* 3, 14 (2024).
- [6] F. Zhan, R. Chen, Z. Ning, D.-S. Ma, Z. Wang, D.-H. Xu, and R. Wang, Perspective: Floquet engineering topological states from effective models towards realistic materials, *Quantum Front.* 3, 21 (2024).
- [7] G. Ma, M. Xiao, and C. T. Chan, Topological phases in acoustic and mechanical systems, *Nat. Rev. Phys.* 1, 281 (2019).
- [8] H. Xue, Y. Yang, and B. Zhang, Topological acoustics, *Nat. Rev. Mater.* 7, 974 (2022).
- [9] Z.-K. Lin, Q. Wang, Y. Liu, H. Xue, B. Zhang, Y. Chong, and J.-H. Jiang, Topological phenomena at defects in acoustic, photonic and solid-state lattices, *Nat. Rev. Phys.* 5, 483 (2023).
- [10] T. Shah, C. Brendel, V. Peano, and F. Marquardt, Colloquium: Topologically protected transport in engineered mechanical systems, *Rev. Mod. Phys.* 96, 021002 (2024).
- [11] Y. Liu, K. Li, W. Liu, Z. Zhang, Y. Cheng, and X. Liu, Observation of chiral Landau levels in two-dimensional acoustic system, *Quantum Front.* 3, 26 (2024).
- [12] N. R. Cooper, J. Dalibard, and I. B. Spielman, Topological bands for ultracold atoms, *Rev. Mod. Phys.* 91, 015005 (2019).
- [13] M. C. Rechtsman, J. M. Zeuner, Y. Plotnik, Y. Lumer, D. Podolsky, F. Dreisow, S. Nolte, M. Segev, and A. Szameit, Photonic Floquet topological insulators, *Nature* 496, 196 (2013).
- [14] T. Ozawa, H. M. Price, A. Amo, N. Goldman, M. Hafezi, L. Lu, M. C. Rechtsman, D. Schuster, J. Simon, O. Zilberberg, and I. Carusotto, Topological Photonics, *Rev. Mod. Phys.* 91, 015006 (2019).
- [15] M. Kim, Z. Jacob, and J. Rho, Recent advances in 2D, 3D and higher-order topological photonics, *Light: Science & Applications* 9, 1 (2020).
- [16] M. Yang, J.-S. Xu, C.-F. Li, and G.-C. Guo, Simulating topological materials with photonic synthetic dimensions in cavities, *Quantum Front.* 1, 10 (2022).
- [17] D. Smirnova, D. Leykam, Y. Chong, and Y. Kivshar, Nonlinear topological photonics, *Appl. Phys. Rev.* 7, 021306 (2020).
- [18] A. Szameit and M. C. Rechtsman, Discrete nonlinear topological photonics, *Nat. Phys.* 20, 905 (2024).
- [19] M. J. Ablowitz, C. W. Curtis, and Y.-P. Ma, Linear and nonlinear traveling edge waves in optical honeycomb lattices, *Phys. Rev. A* 90, 023813 (2014).
- [20] D. Leykam and Y. D. Chong, Edge Solitons in Nonlinear-Photonic Topological Insulators, *Phys. Rev. Lett.* 117, 143901 (2016).
- [21] Y. Lumer, M. C. Rechtsman, Y. Plotnik, and M. Segev, Instability of bosonic topological edge states in the presence of interactions, *Phys. Rev. A* 94, 021801 (2016).
- [22] Y. V. Kartashov and D. V. Skryabin, Modulational instability and solitary waves in polariton topological insulators, *Optica* 3, 1228 (2016).
- [23] Y. V. Kartashov and D. V. Skryabin, Bistable Topological Insulator with Exciton-Polaritons, *Phys. Rev. Lett.* 119, 253904 (2017).
- [24] D. A. Dobrykh, A. V. Yulin, A. P. Slobozhanyuk, A. N. Poddubny, and Yu. S. Kivshar, Nonlinear Control of Electromagnetic Topological Edge States, *Phys. Rev. Lett.* 121, 163901 (2018).
- [25] W. Zhang, X. Chen, Y. V. Kartashov, V. V. Konotop, and F. Ye, Coupling of Edge States and Topological Bragg Solitons, *Phys. Rev. Lett.* 123, 254103 (2019).
- [26] D. A. Smirnova, L. A. Smirnov, D. Leykam, and Y. S. Kivshar, Topological Edge States and Gap Solitons in the Nonlinear Dirac Model, *Laser & Photonics Reviews* 13, 1900223 (2019).
- [27] Y.-L. Tao, N. Dai, Y.-B. Yang, Q.-B. Zeng, and Y. Xu, Hinge solitons in three-dimensional second-order topological insulators, *New J. Phys.* 22, 103058 (2020).
- [28] M. Guo, S. Xia, N. Wang, D. Song, Z. Chen, and J. Yang, Weakly nonlinear topological gap solitons in Su-Schrieffer-Heeger photonic lattices, *Opt. Lett.* 45, 6466 (2020).
- [29] Z. Zhang, R. Wang, Y. Zhang, Y. V. Kartashov, F. Li,

- H. Zhong, H. Guan, K. Gao, F. Li, Y. Zhang, and M. Xiao, Observation of edge solitons in photonic graphene, *Nat. Commun.* 11, 1902 (2020).
- [30] S. Mukherjee and M. C. Rechtsman, Observation of Unidirectional Solitonlike Edge States in Nonlinear Floquet Topological Insulators, *Phys. Rev. X* 11, 041057 (2021).
- [31] T. Tuloop, R. W. Bomantara, C. H. Lee, and J. Gong, Nonlinearity induced topological physics in momentum space and real space, *Phys. Rev. B* 102, 115411 (2020).
- [32] M. S. Kirsch, Y. Zhang, M. Kremer, L. J. Maczewsky, S. K. Ivanov, Y. V. Kartashov, L. Torner, D. Bauer, A. Szameit, and M. Heinrich, Nonlinear second-order photonic topological insulators, *Nature Phys.* 17, 995 (2021).
- [33] H. Zhong, V. O. Kompanets, Y. Zhang, Y. V. Kartashov, M. Cao, Y. Li, S. A. Zhuravitskii, N. N. Skryabin, I. V. Dyakonov, A. A. Kalinkin, S. P. Kulik, S. V. Chekalin, and V. N. Zadkov, Observation of nonlinear fractal higher order topological insulator, *Light: Science & Applications* 13, 264 (2024).
- [34] B. A. Malomed, Prediction and observation of topological modes in fractal nonlinear optics, *Light: Science & Applications* 14, 29 (2025).
- [35] N. Pernet, P. St-Jean, D. D. Solnyshkov, G. Malpuech, N. C. Zambon, Q. Fontaine, B. Real, O. Jamadi, A. Lemaitre, M. Morassi, L. L. Gratiot, T. Baptiste, A. Harouri, I. Sagnes, A. Amo, S. Ravets, and J. Bloch, Gap solitons in a one-dimensional driven-dissipative topological lattice, *Nature Phys.* 18, 678 (2022).
- [36] M. Ezawa, Nonlinearity-induced chiral solitonlike edge states in Chern systems, *Phys. Rev. B* 106, 195423 (2022).
- [37] Y. V. Kartashov, A. A. Arkhipova, S. A. Zhuravitskii, N. N. Skryabin, I. V. Dyakonov, A. A. Kalinkin, S. P. Kulik, V. O. Kompanets, S. V. Chekalin, L. Torner, and V. N. Zadkov, Observation of Edge Solitons in Topological Trimer Arrays, *Phys. Rev. Lett.* 128, 093901 (2022).
- [38] C. Li and Y. V. Kartashov, Topological gap solitons in Rabi Su-Schrieffer-Heeger lattices, *Phys. Rev. B* 108, 184301 (2023).
- [39] M. Ezawa, Nonlinearity-induced transition in the nonlinear Su-Schrieffer-Heeger model and a nonlinear higher-order topological system, *Phys. Rev. B* 104, 235420 (2021).
- [40] F. Lederer, G. I. Stegeman, D. N. Christodoulides, G. Assanto, M. Segev, and Y. Silberberg, Discrete solitons in optics, *Phys. Rep.* 463, 1 (2008).
- [41] Z. Chen, M. Segev, and D. N. Christodoulides, Optical spatial solitons: historical overview and recent advances, *Rep. Prog. Phys.* 75, 086401 (2012).
- [42] Y. V. Kartashov, B. A. Malomed, and L. Torner, Solitons in nonlinear lattices, *Rev. Mod. Phys.* 83, 247 (2011).
- [43] S. Suntsov, K. G. Makris, D. N. Christodoulides, G. I. Stegeman, A. Haché, R. Morandotti, H. Yang, G. Salamo, and M. Sorel, Observation of Discrete Surface Solitons, *Phys. Rev. Lett.* 96, 063901 (2006).
- [44] E. Kengne, W.-M. Liu, L. Q. English, and B. A. Malomed, Ginzburg-Landau models of nonlinear electric transmission networks, *Phys. Rep.* 982, 1 (2022).
- [45] L. Lu, Topology on a breadboard, *Nature Phys.* 14, 875-877 (2018).
- [46] C. H. Lee, S. Imhof, C. Berger, F. Bayer, J. Brehm, L. W. Molenkamp, T. Kiessling, and R. Thomale, Topoelectrical Circuits, *Commun. Phys.* 1, 39 (2018).
- [47] E. Zhao, Topological circuits of inductors and capacitors, *Annals of Physics* 399, 289 (2018).
- [48] J. Dong, V. Juričić, and B. Roy, Topoelectric circuits: Theory and construction, *Phys. Rev. Research* 3, 023056 (2021).
- [49] H. Yang, L. Song, Y. Cao, and P. Yan, Circuit realization of topological physics, *Physics Reports* 1093, 1 (2024).
- [50] H. Sahin, M. B. A. Jalil, and C. H. Lee, Topoelectrical circuits—Recent experimental advances and developments, *APL Electronic Devices* 1, 021503 (2025).
- [51] H. Sahin, Z. B. Siu, S. M. Rafi-Ul-Islam, J. F. Kong, M. B. A. Jalil, and C. H. Lee, Impedance responses and size-dependent resonances in topoelectrical circuits via the method of images, *Phys. Rev. B* 107, 245114 (2023).
- [52] R. Thomale, Dissipative synthetic topological matter: the new frontier, *Front. Phys.* 20, 44602 (2025).
- [53] X. Zheng, T. Chen, W. Zhang, H. Sun, and X. Zhang, Exploring topological phase transition and Weyl physics in five dimensions with electric circuits, *Phys. Rev. Research* 4, 033203 (2022).
- [54] Y. Wang, H. M. Price, B. Zhang, and Y. D. Chong, Circuit implementation of a four-dimensional topological insulator, *Nat. Commun.* 11, 2356 (2020).
- [55] S. Imhof, C. Berger, F. Bayer, J. Brehm, L. W. Molenkamp, T. Kiessling, F. Schindler, C. H. Lee, M. Greiter, T. Neupert, and R. Thomale, Topoelectrical-circuit realization of topological corner modes, *Nature Phys.* 14, 925 (2018).
- [56] S. Liu, S. Ma, Q. Zhang, L. Zhang, C. Yang, O. You, W. Gao, Y. Xiang, T. J. Cui, and S. Zhang, Octupole corner state in a three-dimensional topological circuit, *Light: Science & Applications* 9, 145 (2020).
- [57] T. Helbig, T. Hofmann, S. Imhof, M. Abdelghany, T. Kiessling, L. W. Molenkamp, C. H. Lee, A. Szameit, M. Greiter, and R. Thomale, Generalized bulk-boundary correspondence in non-Hermitian topoelectrical circuits, *Nature Phys.* 16, 747 (2020).
- [58] S. Liu, R. Shao, S. Ma, L. Zhang, O. You, H. Wu, Y. J. Xiang, T. J. Cui, and S. Zhang, Non-Hermitian Skin Effect in a Non-Hermitian Electrical Circuit, *Research* 2021, 5608038 (2021).
- [59] D. Zou, T. Chen, W. He, J. Bao, C. H. Lee, H. Sun, and X. Zhang, Observation of Hybrid Higher-Order Skin-Topological Effect in Non-Hermitian Topoelectrical Circuits, *Nat. Commun.* 12, 7201 (2021).
- [60] M. Yang and C. H. Lee, Percolation-Induced PT Symmetry Breaking, *Phys. Rev. Lett.* 133, 136602 (2024).
- [61] R. Li, W. Wang, X. Kong, B. Lv, Y. Jia, H. Tao, P. Li, and Y. Liu, Realization of a non-Hermitian Haldane model in circuits, *Front. Phys.* 20, 44204 (2025).
- [62] J. Wu, Z. Wang, Y. Biao, F. Fei, S. Zhang, Z. Yin, Y. Hu, Z. Song, T. Wu, F. Song, and R. Yu, Non-Abelian Gauge Fields in Circuit Systems, *Nature Electron.* 5, 635 (2022).
- [63] Q. Guo, T. Jiang, R.-Y. Zhang, L. Zhang, Z.-Q. Zhang, B. Yang, S. Zhang, and C. T. Chan, Experimental Observation of Non-Abelian Topological Charges and Edge States, *Nature* 594, 195 (2021).
- [64] W. Zhang, H. Yuan, N. Sun, H. Sun, and X. Zhang, Observation of Novel Topological States in Hyperbolic Lattices, *Nat. Commun.* 13, 2937 (2022).
- [65] W. Zhang, F. Di, X. Zheng, H. Sun, and X. Zhang, Hyperbolic Band Topology with Non-Trivial Second Chern Numbers, *Nat. Commun.* 14, 1083 (2023).
- [66] Y. Hadad, J. C. Soric, A. B. Khanikaev, and A. Alù,

- Self-Induced Topological Protection in Nonlinear Circuit Arrays, *Nature Electron.* 1, 178 (2018).
- [67] Y. Wang, L.-J. Lang, C. H. Lee, B. Zhang, and Y. D. Chong, Topologically Enhanced Harmonic Generation in a Nonlinear Transmission Line Metamaterial, *Nat. Commun.* 10, 1102 (2019).
- [68] F. Zangeneh-Nejad and R. Fleury, Nonlinear Second-Order Topological Insulators, *Phys. Rev. Lett.* 123, 053902 (2019).
- [69] T. Kotwal, F. Moseley, A. Stegmaier, S. Imhof, H. Brand, T. Kießling, R. Thomale, H. Ronellenfitsch, and J. Dunkel, Active Topoelectrical Circuits, *Proc. Natl. Acad. Sci. U.S.A.* 118, e2106411118 (2021).
- [70] H. Hohmann, T. Hofmann, T. Helbig, S. Imhof, H. Brand, L. K. Upreti, A. Stegmaier, A. Fritzsche, T. Müller, U. Schwingenschlögl, C. H. Lee, M. Greiter, L. W. Molenkamp, T. Kießling, and R. Thomale, Observation of Cnoidal Wave Localization in Nonlinear Topoelectrical Circuits, *Phys. Rev. Research* 5, L012041 (2023).
- [71] J. Tang, F. Ma, F. Li, H. Guo, and D. Zhou, Strongly Nonlinear Topological Phases of Cascaded Topoelectrical Circuits, *Front. Phys.* 18, 33311 (2023).
- [72] H. Sahin, H. Akgün, Z. B. Siu, S. M. Rafi-Ul-Islam, J. F. Kong, M. B. A. Jalil, and C. H. Lee, Protected Chaos in a Topological Lattice, *Adv. Sci.* 12, e03216 (2025).
- [73] R. Li, W. Wang, X. Kong, C. Shang, Y. Jia, G.-G. Liu, Y. Liu, and B. Zhang, Self-Induced Topological Edge States in a Lattice with Onsite Nonlinearity, *arXiv:2504.11964*.
- [74] K. Sone and Y. Hatsugai, Topological-to-topological transition induced by on-site nonlinearity in a one-dimensional topological insulator, *arXiv:2501.10087*.
- [75] A. Suntharalingam, L. Fernández-Alcázar, R. Kononchuk, and T. Kottos, Noise resilient exceptional-point voltmeters enabled by oscillation quenching phenomena, *Nat. Commun.* 14, 5515 (2023).
- [76] S. Yu, X. Piao, and N. Park, Neuromorphic Functions of Light in Parity-Time-Symmetric Systems, *Advanced Science* 6, 1900771 (2019).
- [77] S. Yu, X. Piao, and N. Park, Topologically protected optical signal processing using parity-time-symmetric oscillation quenching, *Nanophotonics* 10, 2883 (2021).
- [78] S. Choi, J. Kim, J. Kwak, N. Park, and S. Yu, Topologically Protected All-Optical Memory, *Adv. Elect. Materials* 8, 2200579 (2022).
- [79] S. Mandal, G.-G. Liu, and B. Zhang, Topology with Memory in Nonlinear Driven-Dissipative Photonic Lattices, *ACS Photonics* 10, 147 (2023).
- [80] L. Jin, Topological Phases and Edge States in a Non-Hermitian Trimerized Optical Lattice, *Phys. Rev. A* 96, 032103 (2017).
- [81] V. M. Martinez Alvarez and M. D. Coutinho-Filho, Edge States in Trimer Lattices, *Phys. Rev. A* 99, 013833 (2019).
- [82] R. Li and Y. Hadad, Reduced Sensitivity to Disorder in a Coupled-Resonator Waveguide with Disordered Coupling Coefficients, *Phys. Rev. A* 103, 023503 (2021).
- [83] Y. Wang, Y.-H. Lu, J. Gao, Y.-J. Chang, H. Tang, and X.-M. Jin, Experimental Topological Photonic Superlattice, *Phys. Rev. B* 103, 014110 (2021).
- [84] A. Anastasiadis, G. Styliaris, R. Chaunsali, G. Theocharis, and F. K. Diakonov, Bulk-Edge Correspondence in the Trimer Su-Schrieffer-Heeger Model, *Phys. Rev. B* 106, 085109 (2022).
- [85] Y. Hadad, V. Vitelli, and A. Alù, Solitons and Propagating Domain Walls in Topological Resonator Arrays, *ACS Photonics* 4, 1974 (2017).
- [86] K. Sone, M. Ezawa, Y. Ashida, N. Yoshioka, and T. Sagawa, Nonlinearity-induced topological phase transition characterized by the nonlinear Chern number, *Nat. Phys.* 20, 1164 (2024).
- [87] C. Li and Y. V. Kartashov, Stable Vortex Solitons Sustained by Localized Gain in a Cubic Medium, *Phys. Rev. Lett.* 132, 213802 (2024).
- [88] R. Li, X. Kong, W. Wang, Y. Jia, and Y. Liu, Newton conjugate gradient method for discrete nonlinear Schrödinger equations, *Chaos, Solitons & Fractals* 195, 116302 (2025).

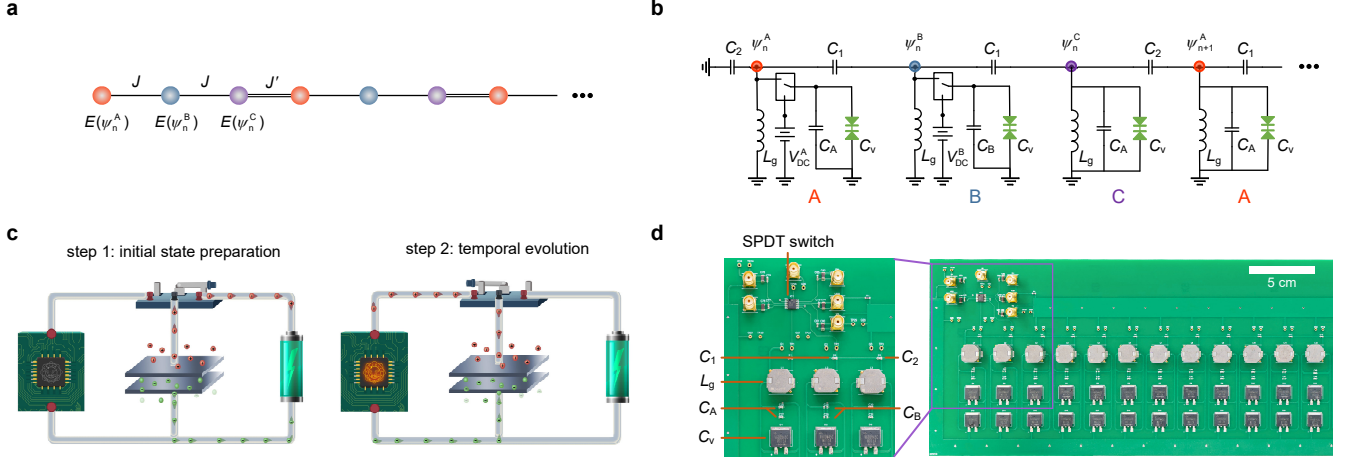


FIG. 1. The implementation of the nonlinear trimer EC lattice and the realization of quench dynamics. **a:** The schematic of the nonlinear trimer lattice, where J and J' represent the intra- and inter-cell hopping amplitudes, respectively, and onsite energy E at each site depends on the wave function of that site, $\psi_n^{A,B,C}$. **b:** The circuit implementation of the nonlinear trimer lattice, where the node voltages correspond to the wave functions at the lattice sites, capacitors C_1 and C_2 emulate the intra- and inter-cell hopping amplitudes, respectively. The onsite nonlinearity is provided by the common-cathode diodes, which exhibit voltage-dependent capacitance C_v . In the two leftmost nonlinear LC oscillators, SPDT switches and DC voltage sources are employed to implement the quench dynamics. **c:** The illustration of the quench dynamics, which involves two steps, *viz.*, the preparation of the initial state and its subsequent time evolution. The charging of capacitors and diodes corresponds to the preparation of the initial state, while the discharging represents the evolution in the EC lattice. **d:** The experimental sample of the nonlinear trimer EC lattice. The inset shows an enlarged fragment with typical circuit components. Experimentally, we use two common-cathode diodes connected in parallel to provide the capacitance C_v .

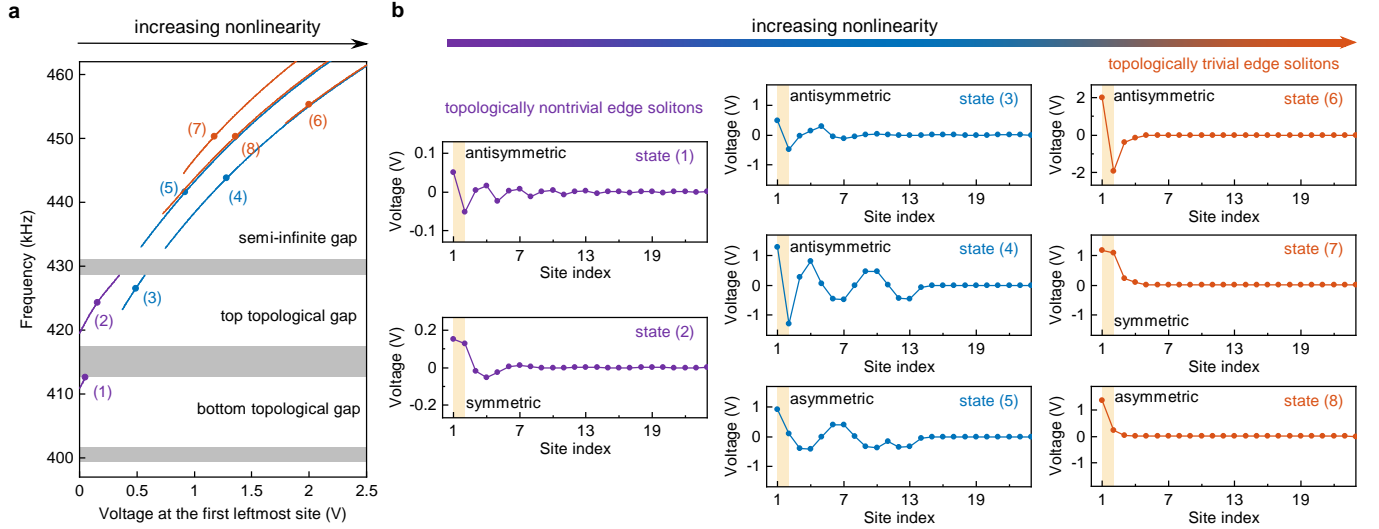


FIG. 2. Frequency spectra and typical profiles of edge solitons. **a:** The frequency spectra as a function of the voltage at the first leftmost site ψ_1^A . The shaded regions represent the underlying spectra of the linear bulk bands. The three bandgaps, *viz.*, the semi-infinite gap, top topological gap, and bottom topological gap, are defined with respect to the linear bulk spectra. In the case of weak nonlinearity, two topologically nontrivial edge solitons (purple branches) originate from the linear topological edge states. As the voltage increases, distinct families of edge solitons emerge (blue branches). When nonlinearity is sufficiently strong, the topologically trivial edge solitons emerge (orange branches). **b:** Profiles of the edge solitons which are indicated by numbers (1)-(8) in (a). The edge solitons are labeled as “antisymmetric”, “symmetric”, or “asymmetric” based on the internal structures at the two leftmost sites (indicated by yellow bars). The states in the first and third columns correspond to the topologically nontrivial and trivial edge solitons, respectively.

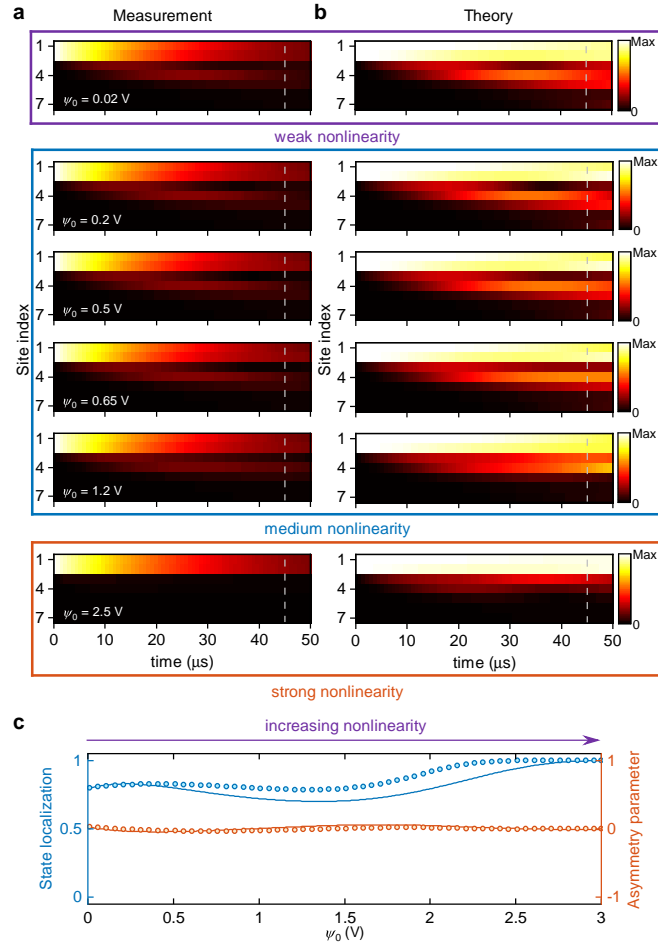


FIG. 3. **The quench dynamics initiated by the out-of-phase excitations.** **a** and **b**: The experimentally observed and theoretically predicted evolution initiated by different initial voltage excitations. **c**: The state localization and asymmetry parameter, defined as per Eqs. (4) and (5), respectively, as extracted from the voltage distributions at $t = 45 \mu\text{s}$ [this time moment is indicated by the dashed lines in (a)-(b)]. The continuous curves and chains of circles denote the theoretical and experimental results, respectively.

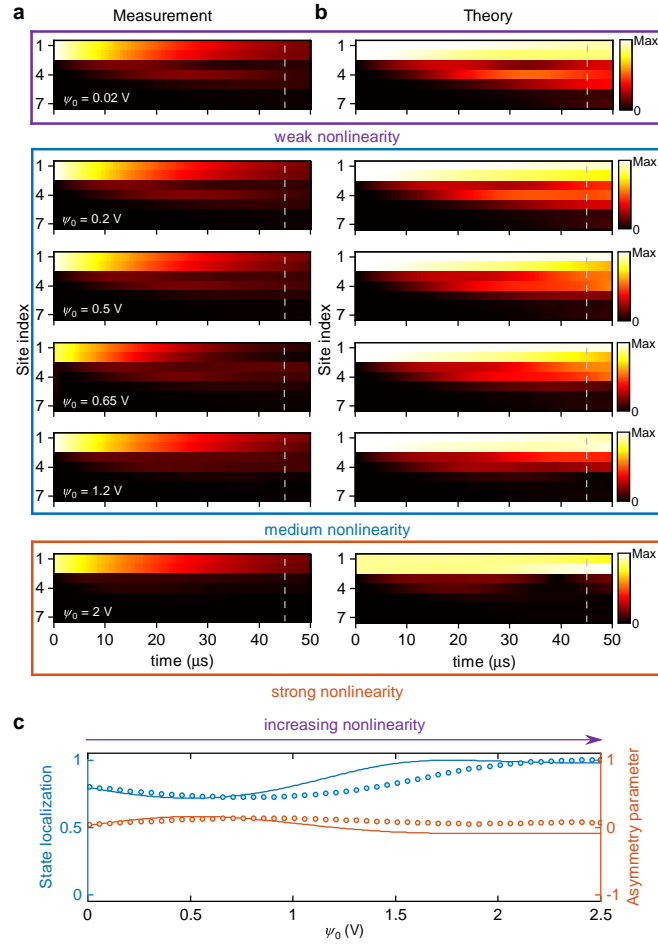


FIG. 4. **The quench dynamics initiated by the in-phase excitations.** **a** and **b**: The experimentally observed and theoretically predicted evolution initiated by different initial voltage excitations. **c**: The state localization and asymmetry parameter, defined as per Eqs. (4) and (5), respectively, as extracted from the voltage distributions at $t = 45 \mu\text{s}$ [this time moment is indicated by the dashed lines in (a)-(b)]. The continuous curves and chains of circles denote the theoretical and experimental results, respectively.

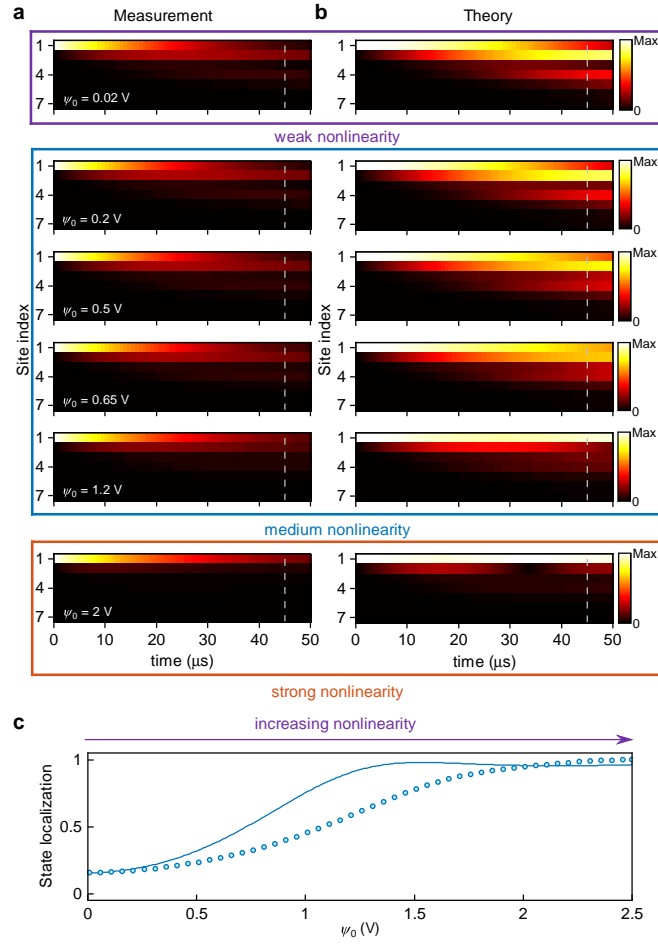


FIG. 5. **The quench dynamics initiated by the single-site excitations.** **a** and **b**: The experimentally observed and theoretically predicted evolution initiated by different initial voltage excitations. **c**: The state localization parameter defined as per Eq. (7), as extracted from the voltage distributions at $t = 45\text{ }\mu\text{s}$ [this time moment is indicated by the dashed lines in (a)-(b)]. The continuous curve and chain of circles denote the theoretical and experimental results, respectively.